RSC Advances

COMMUNICATION

View Article Online
View Journal | View Issue

Cite this: *RSC Adv.*, 2014, **4**, 60106

On the graphene incorporated $LiMn_2O_4$ nano-structures: possibilities for tuning the preferred orientations and high rate capabilities

K. Ragavendran,*[a] Xia Hui,*[b] Xiao Gu,[c] Daniel Sherwood,[d] Bosco Emmanuel[d] and Abdul Kariem Arof[a]

Received 20th October 2014
Accepted 3rd November 2014

DOI: 10.1039/c4ra12754d

www.rsc.org/advances

Nano-material synthesis (here: $LiMn_2O_4$) carried out in the presence of graphene nano-sheets is shown using a crystal shape algorithm to be preferentially oriented along the thermodynamically stable (400) direction, indicating that graphene controls the synthesis through a thermo-dynamical step. Electrochemical studies show that the cathode material with preferred orientation along the (400) direction possesses superior electrochemical properties in general and much better rate capability in particular.

Introduction

Besides its applications in the non-conventional energy sector as a catalyst in the photochemical water splitting,[1] super capacitor[2] and as battery cathode material[3] with better cost effectiveness, safety, efficiency and environment benign aspects compared to Li_xCoO_2, the spinel type $Li_xMn_2O_4$ also serves as a prototype compound in the hands of a condensed matter physicist. Its application in the study of charge ordering, frustrated magnetism and geo-physics are available in the literature.[4–6] The motivation for our series of work on $LiMn_2O_4$ crystal habits[7–9] arose from an article by Chen *et al.* that the desert rose morphology of $LiCoO_2$ [10] showed high rate performance. We found that Chen *et al.* have only used TEM to study the morphology of $LiCoO_2$. On the other hand, almost a couple of years earlier to the report by Chen *et al.*, [10] two researchers from our group (B.E and D.S) had developed a mathematical algorithm[11] that quite successfully simulated the crystal habits of materials such as ZnO, Ge, $MnFe_2O_4$, In_2O_3 *etc.* from their corresponding XRD patterns. This mathematical algorithm was reported to possess several advantages in that it could function as a complementary soft tool to provide information on the material morphology that is otherwise not possible using TEM only.

For instance, in the presence of agglomeration of individual crystallites, TEM captures the shapes of only the agglomerates, while the crystal shape algorithm captures the shapes of the crystallites constituting the agglomerate. Furthermore, equipments such as the TEM can provide only projected 2D information and not the complete 3D information. This is because one cannot view the crystals from arbitrary angles, and only the crystal faces exposed to the instrument camera will be accessible for inspection. The crystal shape algorithm on the other hand can capture the complete 3D information of the crystal. A thorough discussion on the merits is made in the original paper[11] reporting the invention of the crystal shape algorithm.

We were thus motivated to use this soft tool to correlate the electrochemical performance of cathode material with the crystal habit. Meanwhile our work on influence of crystal habits of $LiMn_2O_4$ on the battery characteristics were cited and followed by Tang *et al.*[12] in their 2013 Nano Letters where the authors reported very high charging rates (600 C) in $LiMn_2O_4$ nano-tubes with predominant (400) orientation. The academic piece of work on crystal shapes of cathode materials thus seem to possess large technological application, especially when some parts of India in 2012–2013 faced acute power shortage problem and the need for fast rechargeable batteries for UPS applications was sharply realized. Tuning the preferred orientation of the cathode material is thus one of the most promising approaches to engineer the material for very high rate applications. Quite recently X. H.[13] of our group reported high rate capability and cycling stabilities for $LiMn_2O_4$ nano-crystals when it is anchored with low dimensional carbon materials such as graphene nano-sheets. These nano-particles exhibit ~90% capacity retention at the end of 200 cycles for a given C rate, exhibit symmetrical charge/discharge curves and deliver an astoundingly high value of experimental initial capacity

[a]*Center for Ionics, Department of Physics, University of Malaya, Kuala Lumpur, 50603, Malaysia. E-mail: raguphys@gmail.com*

[b]*School of Materials Science and Engineering, Nanjing University of Science and Technology, Xiaolingwei 200, Nanjing, Jiangsu 210094, P. R. China. E-mail: jasonxiahui@gmail.com*

[c]*Lab for Computational Physical Sciences (Ministry of Education), Fudan University, Shanghai 200433, P. R. China*

[d]*Modeling and Simulation Group, Central Electrochemical Research Institute, Karaikudi 630006, Tamilnadu, India*

(137 mA h^{-1}) compared to ~126 mA h g^{-1} reported so far for $LiMn_2O_4$. An understanding on the mechanism, by which graphene nano-sheets bring about such beneficial properties, would be necessary to design more efficient cathode materials for high rate applications.

Experimental and computational procedures

The experimental[13] and computational[9] procedures adopted in this paper are discussed in detail in the our corresponding references cited above. Nevertheless, we will brief out those procedures in this section. For the typical one step hydrothermal synthesis, 0.020 g graphene nano-sheets were dispersed in 20 cm^3 deionized water and ultrasonicated for 2 h. After that, 0.084 g LiOH and 1 cm^3 ethanol were added and the solution further stirred for 1 h. Finally the stirred solution was transferred into a 30 cm^3 Teflon-lined stainless steel autoclave. The autoclave was sealed and put into an electric oven at 180 °C for 5 h. After the hydrothermal treatment, the produced nanocrystalline $LiMn_2O_{4\ (GNS)}$ was collected by filtration and dried at 90 °C for 12 h. For comparative purpose, pure $LiMn_2O_4$ nanoparticles were also prepared by the hydrothermal method without using GNS and was labeled as $LiMn_2O_{4\ (pristine)}$. Electrochemical measurements on the synthesized cathode materials were carried out using Swagelok cells on Neware Battery system. The positive electrode was a composite of 90 wt% cathode material and 10 wt% PVDF binder for $LiMn_2O_{4\ (GNS)}$ and 70 wt% cathode material 20 wt% carbon black and 10 wt% PVDF binder for $LiMn_2O_{4\ (pristine)}$. The respective composites were dissolved in *N*-methyl pyrrolidone (NMP) solvent and coated over an Al foil and dried 120 °C for 12 hours in vacuum. Crystal shapes of the as synthesized cathode materials were observed using HR-TEM (HR TEM, JEOL, JEM-2010).

The computational part was carried out using the crystal shape algorithm[11] developed by one of our co-authors: Bosco Emmanuel. The crystal shape algorithm was used to ascertain the predominant *hkl* orientations in the cathode material. The mathematical basis of the algorithm and its advantages are dealt with in detail in the original paper.[11] The idea is to construct a mathematical envelope by taking into consideration the real points of intersection and neglecting the virtual points of intersection. Parameters from the X-ray diffraction pattern of the material, whose crystal shape has to be studied, are provided as the inputs. The algorithm then uses the Scherrer formula to provide a set of polygons spanning the crystal boundary oriented in space according to their Miller indices.

It is important to point out that Langford *et al.*[14] and Vargas *et al.*[15] reported, respectively, that the Scherrer constant may depend on the {*hkl*} and on the crystal shape also. In our earlier report[9] we had addressed this issue by studying the crystal habit of $LiMn_2O_4$ by deliberately varying the value of the Scherrer constant (from 0.9 to 1.2). Interestingly it was found that the shape and the predominant orientations were invariant to the variation in the Scherrer constant. However, a scaling effect, wherein a consistent increase in the computed areas of exposure of the *hkl* planes was observed when a higher value of the Scherrer constant was used. However, it was interesting to note that the ratio of the area of exposure of the different *hkl* planes remained the same irrespective of the value of the Scherrer constant used. Following these results, a Scherrer constant value of 1.1 was used in the computations. DFT + *U* as implemented in CASTEP,[16] with an *U* value of +5 eV (ref. 17) was used to compute the relative thermodynamic stabilities of the *hkl* orientations of the cathode material.

Results and discussion

Low dimensional carbon (graphene) templated hydrothermal synthesis of $LiMn_2O_4$ nano-crystals produces phase pure material that could be indexed to the JCPDS (35-0782) of spinel type $LiMn_2O_4$ (Fig. 1(a)). The XRD pattern shows a maximum intensity for the (400) orientation in $LiMn_2O_{4\ (pristine)}$ while it is much lower for $LiMn_2O_{4\ (GNS)}$. However the intensity alone does not give a measure for the predominance along a given *hkl* direction. The product of the intensity and the FWHM is a measure of the diffraction intensity originating from a set of Miller planes having a particular *hkl* or 2θ value. However, this intensity does not tell about the extent to which this *hkl* plane should be exposed in the crystal shape. Because other *hkl* planes may cut across the given *hkl* plane which is then buried without being exposed. On the other hand, the crystal shape is determined by the thicknesses of the crystallite perpendicular to the different *hkl* planes and how these perpendicular directions are inclined with respect to one another. It is a complex interplay of geometry.[9,11] Thus, we shall see in our subsequent discussions that it is the $LiMn_2O_{4\ (GNS)}$ that is predominantly oriented along the thermodynamically most stable (400) direction.

Fig. 1(b) and (c) shows the crystal shapes of $LiMn_2O_{4\ (GNS)}$ and $LiMn_2O_{4\ (pristine)}$ nano-particles as recorded using a high resolution Transmission Microscope (HR-TEM). Most of the particles are seen in a cuboidal shape and this observation is in agreement with the crystal shape generated by the crystal shape algorithm, which is provided as an outset to the respective TEM images. Further the crystal shape algorithm quantifies that the nature of the *hkl* orientations that make the $LiMn_2O_4$ cuboids are the same for both $LiMn_2O_{4\ (GNS)}$and $LiMn_2O_{4\ (pristine)}$, however the (400) orientation which is thermodynamically the most stable *hkl* direction is predominantly expressed in $LiMn_2O_{4\ (GNS)}$.

Table 1 provides the surface energies of the various *hkl* planes in $LiMn_2O_4$ as computed using CASTEP of the Accelrys group. Table 2 shows the extent of exposure of the different *hkl* planes, in $LiMn_2O_{4\ (pristine)}$ and $LiMn_2O_{4\ (GNS)}$, as generated by the crystal shape algorithm. The tabulated information in Tables 1 and 2 is pictorially represented in Fig. 2a and b. From the figures, it is evident that the (400) plane is thermodynamically the most stable orientation (Fig. 2a) in $LiMn_2O_4$ and that it is predominantly expressed in $LiMn_2O_{4\ (GNS)}$ as compared to $LiMn_2O_{4\ (pristine)}$ (Fig. 2b).

During the hydrothermal synthesis of pristine $LiMn_2O_4$ nano-particles, the nucleating centers for the nano-particle growth are placed quite close to each other (Fig. 3a). Nano-

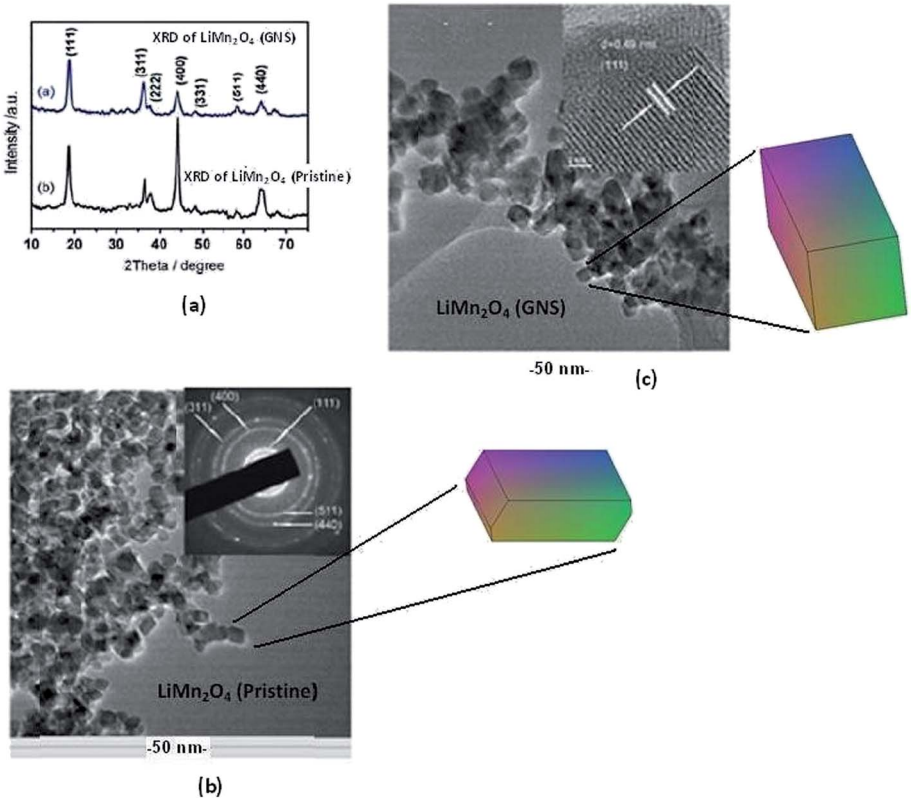

Fig. 1 (a) XRD patterns of $LiMn_2O_4$ nano-material synthesized with graphene nano-sheets ($LiMn_2O_{4\ (GNS)}$) and the nano-material synthesized without graphene nano-sheets ($LiMn_2O_{4\ (pristine)}$). (b). TEM image of $LiMn_2O_{4\ (pristine)}$, the crystal shape of the material generated by the crystal shape algorithm from the corresponding XRD data, is shown as an outset. (c). TEM image of $LiMn_2O_{4\ (GNS)}$ crystal shape studies on the nano-material synthesized without graphene nano-sheets ($LiMn_2O_{4\ (pristine)}$), the crystal shape of the material generated by the crystal shape algorithm from the corresponding XRD data, is shown as an outset. The TEM and XRD figures are adapted with permission from ref. 13. Copyright 2014, Elsevier BV.

crystallization in this case thus occurs under the influence of intermolecular forces, especially the Casimir type of forces which are well known to operate among nano-particles. The Casimir interactions induce the kinetic step in the nano-particle synthesis. On the other hand, when the nano-material synthesis is carried out in the presence of graphene nano-sheets, the graphene nano-sheets with their unique property of large surface area and with their ability to prevent agglomeration among particles, keep the nucleating sites well separated from each other (Fig. 3b). Thus, when nano-material synthesis is carried out in the presence of graphene, intermolecular interactions are minimized and nano-crystallization ($LiMn_2O_4$ in this case) takes place under thermodynamic conditions. $LiMn_2O_{4\ (GNS)}$ is thus predominantly oriented along the thermodynamically stable (400) direction. We will show in the subsequent section that $LiMn_2O_{4\ (GNS)}$ with predominant orientation along the (400) direction possesses better electrochemical characteristics compared to $LiMn_2O_{4\ (pristine)}$.

Fig. 4(a) shows the typical cyclic voltammetric (CV) curves of $LiMn_2O_{4\ (GNS)}$ and $LiMn_2O_{4\ (pristine)}$ electrodes respectively at a scan rate of 0.1 mV s^{-1} in a potential range between 3 and 4.5 V. The first pair of redox peaks at around 4.05/3.94 V correspond to the extraction/insertion of Li^+ ions from/into half of the tetrahedral sites of $LiMn_2O_4$ with Li–Li interaction, while the second

Table 1 Surface energies of the *hkl* planes in $LiMn_2O_4$, computed using DFT + *U* (reproduced with permission from ref. 9, copy right 2014, RSC)[a]

	111	331	400
E (eV)	$-0.45986734 \times 10^{+0.3}$	$-0.73439720 \times 10^{+0.3}$	$-0.32368973 \times 10^{+0.3}$
N	10	16	7
S (Å^2)	29.454	74.126	34.011
$E_{surface}$ (eV Å^{-2})	0.104	0.075	0.037

[a] $E_{surface} = (E - N \times E_{bulk})/2S$, where S is the surface area and $E_{bulk} = -46.59774$ eV.

Table 2 Predominance of the *hkl* planes in $LiMn_2O_4$ synthesized through a hydrothermal method, (a) without and (b) with graphene nano sheets

Method of synthesis	Area (Å^2) of exposure of the (111) plane	Area (Å^2) of exposure of the (331) plane	Area (Å^2) of exposure of the (400) plane
(a) $LiMn_2O_4$ (pristine)	280 000	276 310	49 920
(b) $LiMn_2O_4$ (GNS)	320 000	157 270	160 040

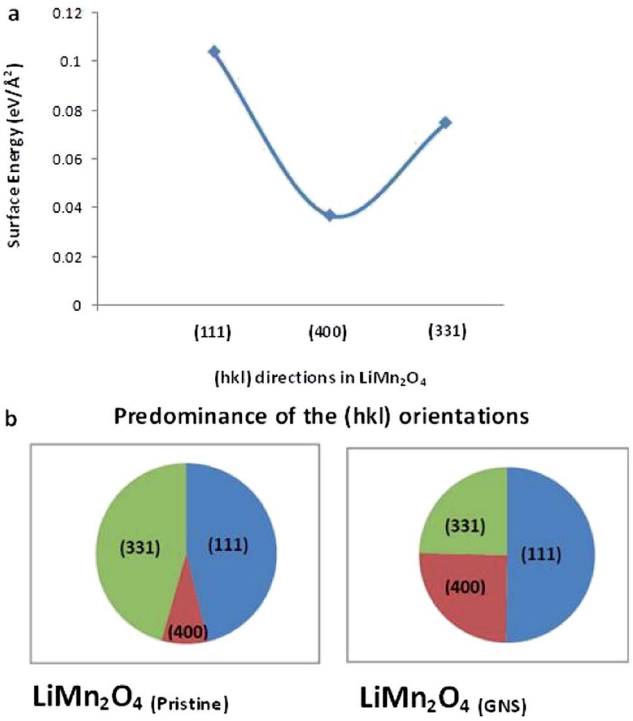

Fig. 2 (a). Surface energies of the various *hkl* directions of spinel $LiMn_2O_4$ as computed using CASTEP using the GGA + *U*. (b). Predominance of the *hkl* orientations in $LiMn_2O_4$ (pristine) and $LiMn_2O_4$ (GNS) as evaluated by the crystal shape algorithm from the corresponding XRD data of the materials.

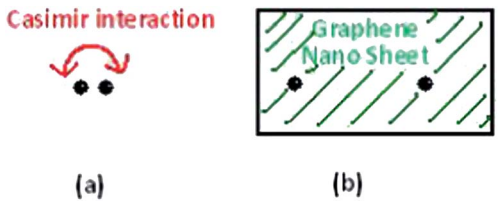

Fig. 3 (a) Nucleating sites in nano-particular $LiMn_2O_4$ (pristine). The nano-structures are close enough to trigger the onset of Casimir type of interactions and thus introducing kinetic control in the material synthesis. (b) Nucleating sites in nano-particular $LiMn_2O_4$ (GNS). Graphene nano-sheets place the nucleating sites in nano-particular $LiMn_2O_4$ (GNS) well separated from each other. Interactions among the nano-particles are thus minimized. This could shift the hydrothermal nano-particular synthesis mechanism towards thermodynamic control.

pair of redox peaks at around 4.17/4.08 V corresponds to the extraction/insertion of Li^+ ions from/into another half of the tetrahedral sites without Li–Li interaction.[18] The potential difference between the cathodic and anodic peaks indicates the polarization of the cell. The cell polarization is induced by the cell resistance, which is mainly contributed by the Li^+ ion transport through the electrode. The CV results in Fig. 4(a) indicate that the $LiMn_2O_4$ (GNS) nano composite electrode represents better kinetics for Li^+ transport.

In Fig. 2b we have already shown that the crystal orientation in $LiMn_2O_4$ (GNS) along the (400) direction is more prominent than that in $LiMn_2O_4$ (pristine). Tang *et al.*[12] has recently reported that $LiMn_2O_4$ with preferred orientation along the (400) direction can have very high rate capability. Since the (400) plane in $LiMn_2O_4$ is the thermodynamically most stable orientation (Fig. 2a), interatomic interactions experienced by a diffusing Li^+ ion along this direction are minimum compared to that experienced by the Li^+ ion while diffusing along other (*hkl*) planes with lower thermodynamical stability. Hence, a cathode material such as the $LiMn_2O_4$ (GNS) with preferred orientation along the (400) direction can be promising for high rate applications.

The first charge/discharge curves of $LiMn_2O_4$ (GNS) and $LiMn_2O_4$ (pristine) electrodes at different C rates are shown in Fig. 4(b) and (c) respectively. The potential separations between the charge and discharge curves of $LiMn_2O_4$ (GNS) electrode (Fig. 4(b)) is much smaller compared to that in $LiMn_2O_4$ (pristine) (Fig. 4(c)), indicating lower polarization in $LiMn_2O_4$ (GNS). The cyclability curves (Fig. 4(d)) at 1 C rate shows that $LiMn_2O_4$ (GNS) exhibits better electrochemical capacity retention (~90% capacity retention after 200 cycles) upon repeated cycling compared to $LiMn_2O_4$ (pristine) (~60% capacity retention after 200 cycles). $LiMn_2O_4$ (GNS) electrode thus exhibits superior cathode material characteristics such as high specific capacity, better cycling stability and rate capability as compared to the $LiMn_2O_4$ (pristine) electrode.

Anchoring the functional material on graphene nano-sheets[19–21] is usually celebrated for improvements in the electrical conductivity, reducing the agglomeration and providing a protective wrap on the active material. In this paper we have shown for the first time the promises of graphene nano-sheets to synthesize nano-materials with preferred orientation. The approach illustrated in this paper, to synthesize $LiMn_2O_4$ nano-material with preferred (400) orientation with improved electrochemical performance, shall as well hold good for tuning the preferred orientations in other functional materials of technological importance.

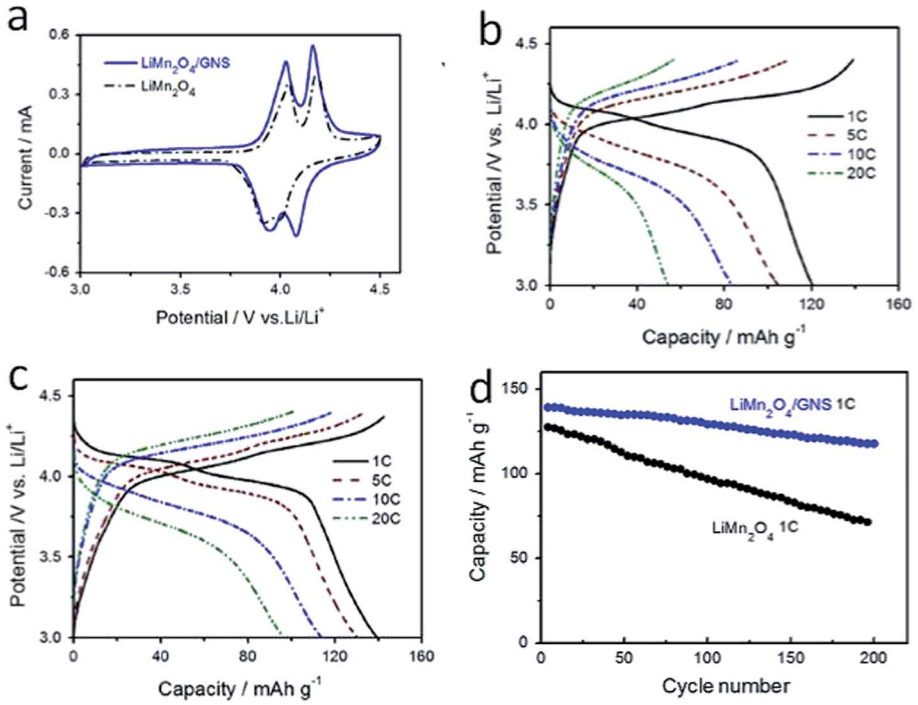

Fig. 4 (a) Cyclic voltammograms of $LiMn_2O_{4\ (pristine)}$ and $LiMn_2O_{4\ (GNS)}$. (b). The first charge/discharge curves of $LiMn_2O_{4\ (Prisine)}$ electrode at different C rates. (c). The first charge/discharge curves of $LiMn_2O_{4\ (GNS)}$ electrode at different C rates. (d). Cycle performance of $LiMn_2O_{4\ (GNS)}$ and $LiMn_2O_{4\ (pristine)}$ electrodes at 1 C rate. The figures are adapted with permission from ref. 13. Copyright 2014, Elseiver BV.

Conclusions

In summary we have shown that graphene nano-sheets serve as a promising approach to tune the predominant *hkl* orientations of nano-materials. These low dimensional carbon materials promote the predominant orientation of the material: here $LiMn_2O_4$, along the thermodynamically stable *hkl* plane: here, the (400) plane, by minimizing the intermolecular interactions at play during the synthesis process. The cathode material synthesis reaction gets controlled through a thermodynamic step. Thus synthesized cathode materials ($LiMn_2O_{4\ (GNS)}$) possess unique electrochemical properties in general and high electrochemical rate capabilities in particular compared to their kinetically controlled cousins ($LiMn_2O_{4\ (pristine)}$).

$LiMn_2O_{4\ (GNS)}$ also possesses a much higher experimental specific capacity ($\sim$137 mA h g^{-1}) compared to $LiMn_2O_{4\ (pristine)}$ with the usual specific capacity of $\sim$126 mA h g^{-1}. This can be understood from the fact that prevention of agglomeration in $LiMn_2O_{4\ (GNS)}$ leads to higher surface area and hence higher electrochemical activity compared to $LiMn_2O_{4\ (pristine)}$ material. Nevertheless, we would also like to point out to an additional possibility that nano-materials synthesized through a thermodynamically controlled step, as in the case of $LiMn_2O_{4\ (GNS)}$, would have a different internal crystal structure compared to those synthesized under kinetically controlled step such as $LiMn_2O_{4\ (pristine)}$. The polymorphism of the material could get tuned when the synthesis is shifted from kinetic towards a thermodynamically controlled step. In other words there is a possibility that $LiMn_2O_{4\ (GNS)}$ is enriched with λ MnO_2, the polymorph which is responsible for electrochemical activity in $LiMn_2O_4$. The high value of initial capacity exhibited by $LiMn_2O_{4\ (GNS)}$ could thus have an intrinsic origin from the internal crystal structure, tuned by a thermodynamically controlled step in its synthesis reaction. Studies on the possible tuning of polymorphism of nano-materials by graphene nano-sheets are underway in our laboratory.

Acknowledgements

This work was financially supported by the NANO-FUND GRANT (53-02-0301089), Malaysia and by the National Natural Science Foundation of China (no. 51102134), the Natural Science Foundation of Jiangsu Province (no. BK20131349), the China Postdoctoral Science Foundation (no. 2013M530258), and Jiangsu Planned Projects for Postdoctoral Research Funds (no. 1202001B).

References

1 D. M. Robinson, Y. B. Go, M. Mui, G. Gardner, Z. Zhang, D. Mastrogiovanni, E. Garfunkel, J. Li, M. Greenblatt and C. Dismukes, *J. Am. Chem. Soc.*, 2013, **135**, 3494.
2 F. X. Wang, S. Y. Xiao, X. W. Gao, Y. S. Zhu, H. P. Zhang, Y. P. Wu and R. Holze, *J. Power Sources*, 2013, **242**, 560.
3 M. M. Thackeray, W. I. F. David, P. G. Bruce and J. B. Goodenough, *Mater. Res. Bull.*, 1983, **18**, 461.
4 J. R. Carvajal, G. Rousse, C. Masquelier and M. Hervieu, *Phys. Rev. Lett.*, 1998, **81**, 4660.

5 R. Basu, C. Felser, A. Maiynan and R. Seshadri, *J. Mater. Chem.*, 2000, **10**, 1921.
6 K. Yamaura, Q. Huang, L. Zhang, K. Takada, Y. Baba, T. Nagai, Y. Matsui, K. Kosuda and E. Takayama-Muromachi, *J. Am. Chem. Soc.*, 2006, **128**, 9448.
7 K. Ragavendran, D. Sherwood, D. Vasudevan and B. Emmanuel, *Phys. B*, 2009, **404**, 2166.
8 K. Ragavendran, H. L. Chou, L. Lu, M. O. Lai, B. J. Hwang, R. Ravikumar, S. Gopukumar, B. Emmanuel, D. Vasudevan and D. Sherwood, *J. Mater. Sci. Eng. B*, 2011, **176**, 1257.
9 K. R. Ragavendran, H. Xia, G. Yang, D. Vasudevan, B. Emmanuel, D. Sherwood and A. K. Arof, *Phys. Chem. Chem. Phys.*, 2014, **16**, 2553.
10 H. L. Chen and C. P. Grey, *Adv. Mater.*, 2008, **20**, 2206.
11 D. Sherwood and B. Emmanuel, *Cryst. Growth Des.*, 2006, **6**, 1415.
12 W. Tang, Y. Hou, W. Faxing, L. Lili, W. Yuping and Z. Kai, *Nano Lett.*, 2013, **13**, 2036.
13 B. Lin, Q. Yin, H. Hu, F. Lu and H. Xia, *J. Solid State Chem.*, 2014, **209**, 23.
14 J. I. Langford and A. J. C. Wilson, *J. Appl. Crystallogr.*, 1978, **11**, 102.
15 R. Vargas, D. Louer and J. I. Langford, *J. Appl. Crystallogr.*, 1983, **16**, 512.
16 M. D. Segall, P. J. D. Lindan, M. J. Probert, C.-J. Pickard, P. J. Hasnip, S. J. Clark and M. C. Payne, *J. Phys.: Condens. Matter*, 2002, **14**, 2717.
17 A. Karim, S. Fosse and K. A. Persson, *Phys. Rev. B: Condens. Matter Mater. Phys.*, 2013, **87**, 075322.
18 M. M. Thackeray, W. I. F. David, P. G. Bruce and J. B. Goodenough, *Mater. Res. Bull.*, 1983, **18**, 461.
19 J. Zhu, D. Yang, Z. Yin, Q. Yan and H. Zhang, *Small*, 2014, **10**, 3480.
20 K. Chang and W. Chen, *Chem. Commun.*, 2011, **47**, 4252.
21 C. N. R. Rao, H. S. S. Ramakrishna Matte and U. Maitra, *Angew. Chem., Int. Ed.*, 2013, **52**, 13162.